Cell-ECM traction force modulates endogenous tension at cell–cell contacts

Venkat Maruthamuthu[a], Benedikt Sabass[b,c], Ulrich S. Schwarz[b,d], and Margaret L. Gardel[a,e,1]

[a]Institute for Biophysical Dynamics, University of Chicago, Chicago, IL 60637; [b]Bioquant, University of Heidelberg, 69120 Heidelberg, Germany; [c]II. Institute for Theoretical Physics, University of Stuttgart, 70550 Stuttgart, Germany; [d]Institute for Theoretical Physics, University of Heidelberg, 69120 Heidelberg, Germany; and [e]James Franck Institute and Department of Physics, University of Chicago, Chicago, IL 60637

Edited by Shu Chien, University of California, San Diego, La Jolla, CA, and approved February 3, 2011 (received for review July 30, 2010)

Cells in tissues are mechanically coupled both to the ECM and neighboring cells, but the coordination and interdependency of forces sustained at cell-ECM and cell–cell adhesions are unknown. In this paper, we demonstrate that the endogenous force sustained at the cell–cell contact between a pair of epithelial cells is approximately 100 nN, directed perpendicular to the cell–cell interface and concentrated at the contact edges. This force is stably maintained over time despite significant fluctuations in cell–cell contact length and cell morphology. A direct relationship between the total cellular traction force on the ECM and the endogenous cell–cell force exists, indicating that the cell–cell tension is a constant fraction of the cell-ECM traction. Thus, modulation of ECM properties that impact cell-ECM traction alters cell–cell tension. Finally, we show in a minimal model of a tissue that all cells experience similar forces from the surrounding microenvironment, despite differences in the extent of cell-ECM and cell–cell adhesion. This interdependence of cell–cell and cell-ECM forces has significant implications for the maintenance of the mechanical integrity of tissues, mechanotransduction, and tumor mechanobiology.

cellular mechanotransduction | cadherin | adherens junctions | focal adhesions | intercellular force transmission

In multicellular tissue, morphological changes during tissue formation, maintenance, and repair require the dynamic regulation and coordination of cellular movements and shape (1). Physical interactions in multicellular populations are, to a large degree, guided by adhesions formed both between neighboring cells and between cells and the ECM (2, 3). Rather than simply playing a passive role in maintaining attachment and resisting external forces, it is becoming increasingly evident that cell-ECM and cell–cell adhesions are also sites of transmission of active, cell-generated forces (4).

The nature of force balance across a cell guides its morphological changes and movement (1). For single cells, integrin-mediated focal adhesions to the ECM sustain large tensile loads generated within the actin cytoskeleton, and these forces regulate cell shape and migration (1, 4, 5). In turn, force-mediated integrin signaling also controls cell growth, proliferation, and differentiation (6, 7). In multicellular ensembles, such as epithelial monolayers, cells form adhesions to neighboring cells, primarily through cadherin-mediated adhesions, as well as to the extracellular matrix. Here, morphological changes are driven by the forces generated and sustained at both cell–cell and cell-ECM adhesions. Although it is known that cadherin-mediated adhesions to neighboring cells share similar characteristics of force-dependent growth and signaling observed at focal adhesions (3, 8, 9) and have the potential to sustain large tensile loads (9, 10), little is known about the magnitude of tension sustained at endogenous cell–cell contacts.

Evidence of mechanical tension sustained at endogenous cell–cell contacts has, to a large degree, relied on mechanical interpretations of cytoskeletal dynamics induced by disruption of a cell–cell contact in a multicellular tissue (11–14). Although this method has provided powerful insights about an otherwise experimentally inaccessible quantity, it requires assumptions of the cellular mechanics and can provide only estimates of relative forces at the cell–cell interface. Traction force microscopy of epithelial monolayers has also provided evidence for cell–cell tension during epithelial sheet migration (15). Recently, direct measurements of the endogenous tension exerted at cell–cell contacts have shown that the magnitude of tension at the cell–cell interface regulates the size of the cell–cell adhesive contact for pairs of endothelial cells where the cell shape is geometrically constrained (16). However, the regulation of the force at a cell–cell adhesion in its native, unconstrained morphology remains unknown. Moreover, although it has been speculated that mechanical "cross-talk" between cell-ECM and cell–cell adhesions may play an important role in guiding cellular rearrangements in a multicellular context (17, 18), the extent to which cell–cell forces are coordinated with cell-ECM forces is less certain.

In this paper, we first consider the minimal model of two epithelial cells adherent to both the ECM and each other with a fully developed cell–cell contact. We determine the nature of the endogenous force at the cell–cell contact to be tensile, directed perpendicular to the cell–cell interface, and concentrated at the contact edges. We find that the ratio of the cell–cell force to the total cell-ECM traction force is remarkably constant across cell pairs despite natural variations in cellular contractility. In turn, we show that perturbations to ECM properties such as biochemical composition or mechanical rigidity, well known to alter cellular traction force, modulate the tension sustained at the cell–cell contact. Thus, tension exerted at focal adhesions is directly correlated to the tension at cell–cell contacts. Finally, consideration of an asymmetric three-cell case shows all cells exert similar levels of forces on their microenvironments, even though the extent of cell–cell and cell-ECM adhesion differs. These results have implications for understanding the mechanical coordination between the tension sustained at focal adhesions and cell–cell adhesions in multicellular tissue.

Results

Traction Force Imbalance Measures Endogenous Force at Cell–Cell Contact. The endogenous force transmitted at a single cell–cell contact between pairs of Madin–Darby canine kidney (MDCK) epithelial cells was determined based on a calculation of the balance of traction forces exerted on the ECM. To assess traction forces exerted at integrin-mediated adhesions, MDCK cells were plated on compliant, collagen-coated polyacrylamide gels suitable for high resolution traction force microscopy (19). Traction force vectors were calculated from the substrate displacement

Author contributions: V.M. and M.L.G. designed research; V.M. performed research; V.M., B.S., and U.S.S. contributed new reagents/analytic tools; V.M., B.S., and U.S.S. analyzed data; and V.M. and M.L.G. wrote the paper.

The authors declare no conflict of interest.

This article is a PNAS Direct Submission.

[1]To whom correspondence should be addressed. E-mail: gardel@uchicago.edu.

This article contains supporting information online at www.pnas.org/lookup/suppl/doi:10.1073/pnas.1011123108/-/DCSupplemental.

vectors by using Fourier transform traction cytometry algorithms (19) (*SI Text*).

In isolated MDCK cells, traction stresses were exerted at the cell periphery and directed toward the cell center (Fig. 1 *A* and *B*); the location of traction stresses corresponds to the typical distribution of focal adhesions in individual cells (Fig. S1) and no colocalization of GFP-E-cadherin to sites of cell-ECM traction was observed (Fig. 1*A*). The traction stress multiplied by the unit grid area yielded the traction force vector, $\vec{T}_i$. The sum of traction force magnitudes across the cell, $\sum|\vec{T}_i|$, provided a measure of the total cell-ECM generated force and was approximately 250 nN (*SI Text*). The vector sum of the traction forces across the cell, $\sum\vec{T}_i$, measured the unbalanced traction force. To compare the magnitude of the unbalanced force to the total cell-ECM force, the ratio $|\sum\vec{T}_i|/\sum|\vec{T}_i|$ was used. For single cells, the unbalanced force was $5 \pm 3\%$ of the total cell-ECM force (Fig. 1*C*). We attribute this small degree of force imbalance to the error of our analysis routines, as real force imbalances of this magnitude would result in rapid acceleration of the cell body (*SI Text*).

Pairs of MDCK cells with fully expanded cell–cell contacts were identified by prominent E-cadherin localization along the cell–cell interface and, in a large fraction of cells, enhanced localization of GFP-E-cadherin in plaques at the edges of the cell–cell contact (20, 21) (Fig. 1*D*). In cell pairs, focal adhesions largely disassembled at regions of cell–cell contacts, but remained at the free cell edge (21) (Fig. S2). Consistent with this, traction stresses exerted by the cell pair were directed centripetally at the cell periphery and no large traction stresses were exerted under sites of prominent GFP-E-cadherin localization (Fig. 1 *D* and *E*). The total cell-ECM force generated by the cell pair was approximately 400 nN, or 200 nN per cell. The traction force vectors were well balanced across the cell pair, and the percent of unbalanced traction force across the cell pair was $5 \pm 3\%$, similar to that observed in single cells (green, Fig. 1*F*).

Using E-cadherin localization to identify the cell–cell boundary, we then calculated the sum of traction force vectors under an individual cell in a cell pair, $\vec{F}_{\text{cell1}} = \sum_{\text{cell1}}\vec{T}_i$ (yellow line, Fig. 1 *D* and *E*; see *SI Text*). This imbalance for a single cell in a cell pair is distinctly larger than the imbalance for the entire cell pair (Fig. 1*F*). Because the cell is in mechanical equilibrium, we deduced that this imbalance reflects the force exerted at the cell–cell interface by its neighbor (schematic, Fig. 1*F*). If this were the case, both cells in the pair would exert equal and opposing forces on each other. Indeed, we observed a strong correlation between the magnitude of the force imbalance vector of the two cells in a cell pair, $|\vec{F}_{\text{cell1}}|$ and $|\vec{F}_{\text{cell2}}|$ (Fig 1*G*). The average endogenous tension exerted at the cell–cell interface was calculated as the vector difference $\vec{F}_{\text{cell-cell}} = (\vec{F}_{\text{cell1}} - \vec{F}_{\text{cell2}})/2$. We found that the magnitude of $\vec{F}_{\text{cell-cell}}$ was broadly distributed, with an average of approximately 100 nN (Fig. 1*H*) and that the direction of the vector was perpendicular to the cell–cell interface (Fig. 1*I*). The magnitude of the vector sum, $|(\vec{F}_{\text{cell1}} + \vec{F}_{\text{cell2}})|/2$, which, in principle, should be zero, provided an estimate of measurement error and was approximately 10% that of $F_{\text{cell-cell}}$. From the uncertainty in single cell traction force balance, we determined the upper bound of $F_{\text{cell-cell}}$ measurement error to be 30% (*SI Text*).

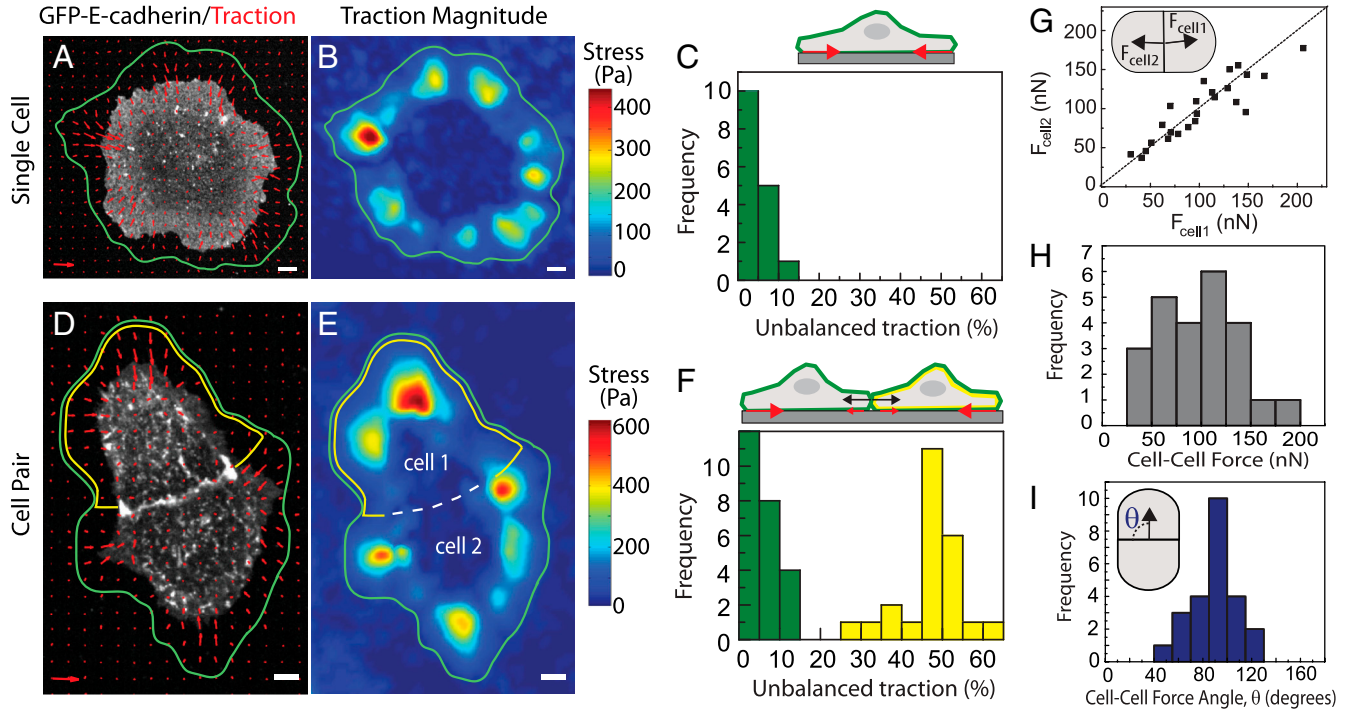

Fig. 1. *Traction force imbalance yields the endogenous cell–cell force.* (*A*) MDCK cell expressing GFP-E-cadherin with traction stress vectors (red arrows) superimposed. Green line indicates region used for calculation of total traction force. Stress magnitude and distance scale are indicated by the red arrow and white line, respectively. (*B*) Heat-scale plot of traction stress magnitudes of the cell shown in *A*. (*C*, *Top*) Schematic of cell on traction gel with traction stress vectors (red arrow). (*Bottom*) Histogram of the unbalanced traction force across an isolated cell, measured as $|\sum\vec{T}_i|/\sum|\vec{T}_i|$, and expressed as a percentage (number of cells = 16). (*D*) A pair of contacting MDCK cells expressing GFP-E-cadherin with traction stress vectors overlaid (red arrows). Outline of the regions used to calculate the force balance within the cell pair or a single cell are indicated by the green and yellow lines, respectively. (*E*) Heat-scale plot of traction stress magnitudes of the cell pair shown in *D*. (*F*, *Top*) Schematic of side view of the cell pair on traction gel with traction stresses (red arrows) and cell–cell forces (black arrows) depicted. (*Bottom*) Histogram of the unbalanced traction force, as measured in *C* for both a cell pair (green) and a single cell within the cell pair (yellow) (number of cell pairs = 24). (*G*) Net force exerted by cell 2 on cell 1, F_{cell1}, as a function of the force exerted by cell 1 on cell 2, F_{cell2}. Dashed line indicates a slope of one. (*Inset*) Schematic of a cell pair depicting F_{cell1} and F_{cell2}. (*H*) Histogram of the endogenous cell–cell force; mean $\pm$ SD is 100 ± 40 nN. (*I*) Histogram of the angle between the cell–cell force and the line joining the edges of the cell–cell contact; mean $\pm$ SD is 88 ± 18^0. (*Inset*) Schematic depicting the angle calculated. Scale bar in *A*, *B*, *D*, and *E* is 5 μm. Reference traction vector in *A* and *D* is 950 Pa.

The method developed here is, in principle, similar to those in recent reports (15, 16), but has been extended to single cell–cell contacts between unconstrained cell pairs on uniform substrates. This method is robust to choice of traction force reconstruction routine and parameters chosen (*SI Text*). Henceforth in this paper, we refer to this way of deducing the endogenous forces at the cell–cell contact as the traction force imbalance method (TFIM).

Cell–Cell Force Is Independent of the Cell–Cell Contact Size and Is Stable During Dynamic Cell Morphological Changes. To explore the regulation of the endogenous tension at cell–cell contacts, we sought correlation of cell–cell force with cadherin localization at the cell–cell contact. We found that the cell–cell force is not correlated to the integrated intensity of E-cadherin localized at the cell–cell contact (Fig. S3), in contrast to correlations observed when the cell–cell contact is formed with geometrical constraints on cell shape (16).

In unconstrained cell pairs, cells undergo random migration, effecting changes in cell morphology and orientation relative to each other over the course of an hour (Fig 2*A* and Movie S1). Over this time, the spatial organization of the traction stresses changes and reflects changes in cell shape and orientation (Fig. 2*B* and Movie S1). To accommodate the changes in cell morphology, the cell–cell contact dynamically remodels with the contact length changing by as much as 30% over the course of an hour (Fig. 2*C* and Fig. S4). However, during this time, the magnitude of the cell–cell force remains constant (Fig. 2*C* and Fig. S4). Thus, we do not observe a correlation between the cell–cell force and contact length (Figs. S3 and S4). These data indicate that, for mature cell–cell contacts in an unconstrained epithelial cell pair, the length of the cell–cell contact does not strongly correlate to the tension at the cell–cell contact.

Cell–Cell Force Acts at Contact Vertices of Cell Pair. One possible explanation for the independence of the cell–cell force on contact length is that forces are unevenly distributed across the contact length, such that a small portion of the contact sustains a large fraction of the load. Immunofluorescence of F-actin and myosin light chain shows that actomyosin bundles are primarily colocalized at the cell periphery at dense E-cadherin plaques (Fig. 2*D* and Fig. S2), consistent with previous reports (21, 22). The E-cadherin-rich plaques at the cell–cell contact edges can be the considered the contact vertices of a cell pair (20) (Fig. S4). The variation in actin intensity along the cell–cell contact could reflect different levels of force transmission along the length of the contact.

TFIM yields the net force vector at the cell–cell contact but not the distribution of forces along the contact length. To provide insight into the nature of the force distribution along the cell–cell contact, cell–cell adhesion along the contact was differentially disrupted. If the forces were primarily concentrated at the contact vertices, perturbation of the contact edges should lead to a disproportionate decrease in the magnitude of the cell–cell force.

To disrupt the cell–cell contact, we exploited the Ca^{2+} dependence of cadherin binding (23). We first determined the cell morphology, traction force, and cell–cell force for cell pairs with mature cell contacts in calcium-containing media. Then, calcium-free media containing a cell-impermeable calcium chelator, BAPTA, was perfused, and changes in the cell morphology, cell–cell contact, traction force, and cell–cell force were monitored. We observed that cell–cell contacts in a cell pair typically began to rupture at the contact edges (Movie S2) within about 10 min of calcium depletion. Rupture of the cell–cell edge was initiated by the retraction of the F-actin and associated E-cadherin plaque at the contact vertices (Fig. 2*E*, black arrows). Over this time, the central region of the cell–cell contact remained intact and the overall length of the cell–cell contact decreased by only 5–10% (Fig. 2 *E* and *F*).

During the first 10 min of calcium depletion, minimal changes were observed in the total cell-ECM traction force, $\sum |\vec{T}_i|$, indicating that the calcium-free media did not have a large effect on integrin-mediated adhesion to the ECM over this time (Fig. 2*F*). As the cell–cell contact began to rupture, traction

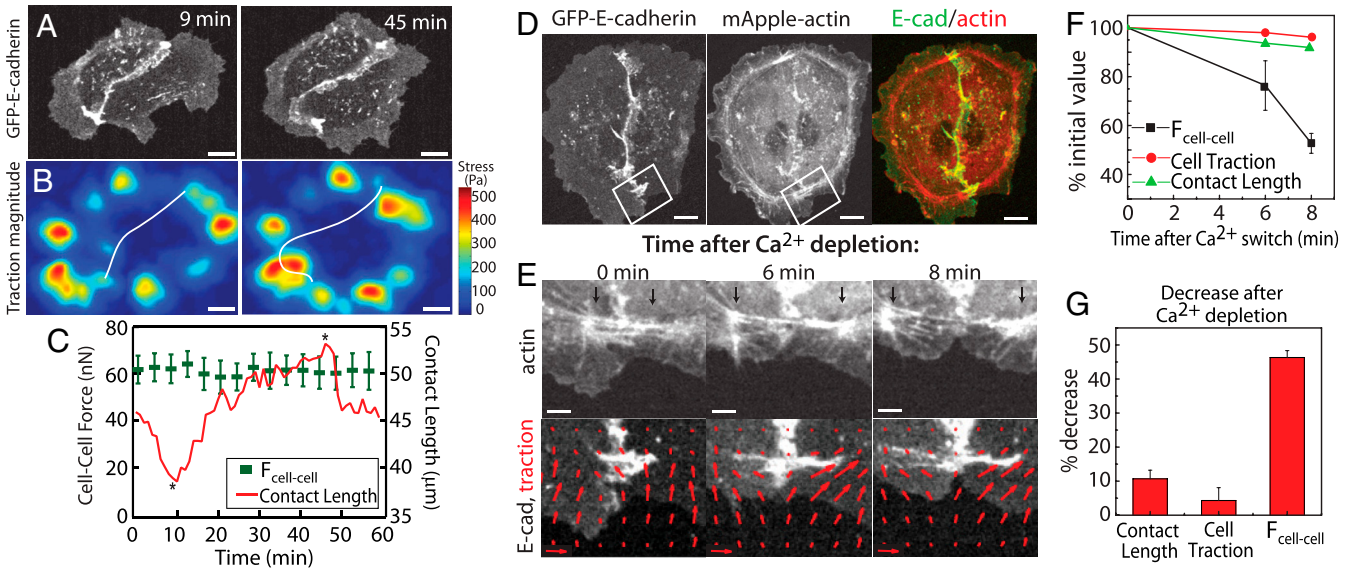

Fig. 2. *Cell–cell force is stable over time and is concentrated at the contact edges.* (*A*) Time lapse images of randomly migrating MDCK cell pair expressing GFP-E-cadherin at times indicated. (*B*) Heat-scale map of traction stress magnitudes of the cell pair at times identical to those in A. Cell–cell contact line indicated by white line. (*C*) Cell–cell force and the cell–cell contact length of a cell pair during time lapse imaging of random migration. Time points corresponding to images in *A* and *B* are denoted by an asterisk (*). (*D*) Localization of GFP-E-cadherin and mApple-actin in an MDCK cell pair. White outline indicates region used for analysis in *E*. (*E*) Images of actin (*Top*) and E-cadherin (*Bottom*) at times after calcium depletion. E-cadherin images overlaid with traction stress vectors (red arrows) at times after calcium depletion. Arrows indicate location of fiducial marks in F-actin coinciding with the edges of the GFP-E-cadherin plaque at the cell–cell contact. Reference traction vector in E is 250 Pa. (*F*) Cell–cell force, total traction force, and cell–cell contact length as a function of time after calcium depletion; data calculated from cell shown in *E*. (*G*) Percentage drop in cell–cell contact length, total traction force, and cell–cell force within 10 min after calcium depletion for $n = 3$ cell pairs. Scale bar in *A*, *B*, and *D* is 10 μm and in *E* is 3 μm.

stresses near the location of the E-cadherin plaque at the contact edges undergoing retraction reoriented away from the cell–cell contact in the direction of retraction (Fig. 2*E*). Over this same time, the cell–cell force significantly dropped, by almost half its initial value (Fig. 2*F*). Thus, as the cell–cell contact disrupted, local traction stresses to the ECM reoriented, thereby leading to a better balance of traction forces in individual cells. Thus, disruption of the peripheral edge of the cell–cell contact, which reduced the contact length and cell-ECM force by less than 10%, reduced the cell–cell force by approximately 50% (Fig. 2*G*). This strongly suggests that the cell–cell forces in a cell pair are inhomogeneously distributed along the cell–cell contact, with a large fraction of the tension transmitted at the peripheral vertices, colocalizing with the heightened E-cadherin, F-actin, and myosin intensities.

Cell–Cell Force Is Proportional to Cell-ECM Traction Force. We sought to closely explore the correlations between the cell–cell force and traction force exerted to the ECM. Our calculation of $F_{\text{cell-cell}}$ reflects a force perpendicular to the cell–cell contact counterbalanced by all traction forces exerted on the ECM in the antiparallel direction, $\sum \vec{T}_{\parallel,i}$ for each cell in the cell pair (Fig. 3*A*). This force balance, however, does not constrain the traction forces that are perpendicular to the cell–cell force vector, $\vec{T}_{\perp,i}$, which are internally balanced (Fig. 3*A*). Thus, the sum of the magnitudes of traction force vectors perpendicular to the cell–cell force, $\sum |\vec{T}_{\perp,i}|$, provided a measure of the tension exerted to the ECM at focal adhesions that is independent of the force balance used to calculate the cell–cell tension.

A broad distribution of the cell-ECM traction force perpendicular to the cell–cell force, $\sum |\vec{T}_{\perp,i}|$ (expressed on a per cell basis) was observed, ranging from 40 to 300 nN, and likely due to natural variation in cellular contractility and cell area. Surprisingly, we found that the cell–cell force, $F_{\text{cell-cell}}$, was directly correlated to $\sum |\vec{T}_{\perp,i}|$ (Fig. 3*B*). As a consequence, $F_{\text{cell-cell}}$ was also tightly correlated to the total cell-ECM traction force, $\sum |\vec{T}_i|$ (Fig. 3*C*). Thus, the ratio between the cell–cell force and cell-ECM traction force per cell for cell pairs was a surprisingly robust constant fraction around 0.5 and remained remarkably constant despite an order of magnitude variation in the traction forces (Fig. 3*D*). This demonstrates a strong correlation between forces transmitted through cell–cell and cell-ECM adhesions.

Although dependence of the cell–cell force on intracellular factors affecting cellular contractility was shown by recent work (16), here we demonstrate an explicit correlation between cellular traction to the ECM and the tensile force exerted at cell–cell contacts. Our results suggest that extracellular factors that perturb cell-ECM traction forces will directly impact forces at cell–cell adhesions.

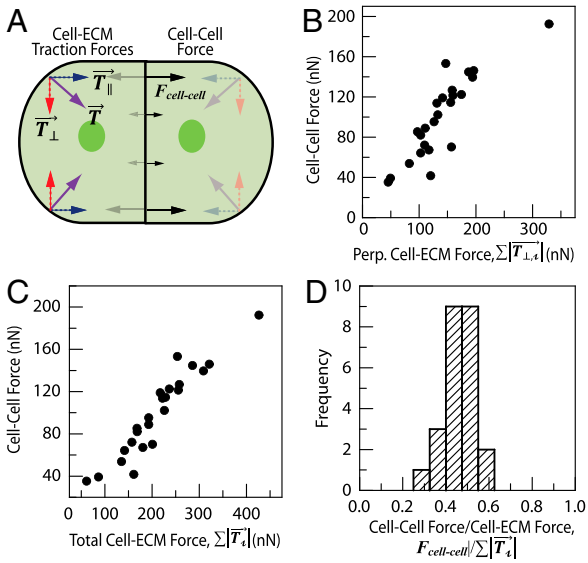

Fig. 3. *Cell–cell force is directly proportional to the total cell-ECM traction force.* (*A*) Schematic of a cell pair depicting force balance between cell-ECM and cell–cell forces. Cell-ECM traction forces acting at cell periphery (purple arrow, $\vec{T}$) can be deconstructed into a component that is parallel (blue arrow, $\vec{T}_{\parallel}$) and perpendicular (red arrow, $\vec{T}_{\perp}$) to the cell–cell force. Cell–cell forces ($\vec{F}_{\text{cell-cell}}$, black arrows) act primarily perpendicular to the cell–cell contact. (*B*) Cell–cell force as a function of the total traction force per cell directed perpendicular to the cell–cell force. Data are for $n = 24$ MDCK cell pairs. (*C*) Cell–cell force as a function of the total traction force exerted per cell. (*D*) Histogram of the ratio of the cell–cell force to the total traction force exerted per cell, mean $\pm$ SD $= 0.47 \pm 0.07$.

ECM Properties Modulate Endogenous Cell–Cell Forces. To test the hypothesis that independently altering the cell-ECM traction forces would affect the cell–cell force, we altered ECM properties known to affect cell-ECM traction forces. Changing the ECM ligand from collagen I (CnI) to fibronectin (Fn), while maintaining a constant ECM stiffness, was previously shown to impact traction force magnitudes in other cell types (24). For MDCK cells plated on Fn-coated matrices, the average cellular traction force decreased approximately 40% to 150 nN (Fig. 4*A*). Remarkably, we found that the average cell–cell force also decreased to 60 nN such that the ratio $F_{\text{cell-cell}}/\sum|\vec{T}_i|$ remained constant (Fig. 4 *B* and *C*).

Increased mechanical rigidity of the ECM, while maintaining a constant ECM ligand, has also been found to enhance cellular traction force (7). With MDCK cells, we found that increasing Young's modulus of the underlying hydrogel from 8.4 to 20.7 kPa enhanced the total cellular traction forces by approximately 25% to 300 nN (Fig. 4*A*). At the same time, we found that the average cell–cell force also proportionately increased to 130 nN and was consistent with the same trend relating cell–cell force and cell-ECM traction observed (Fig. 4 *B* and *C*). These results show that perturbations to the biochemistry or

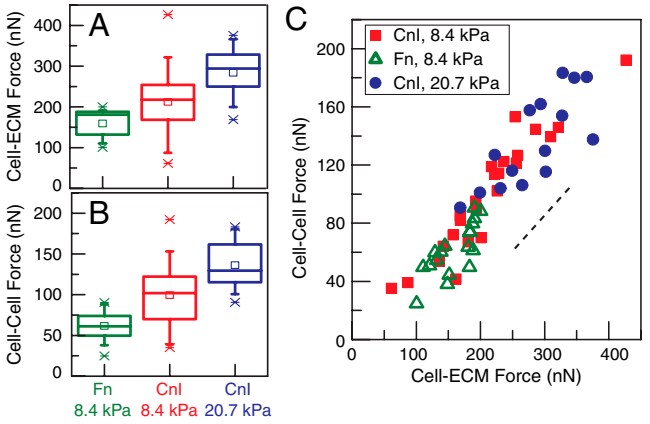

Fig. 4. *ECM properties modulate endogenous cell–cell forces.* (*A*) Box plot of the total cell-ECM traction force for cells plated on substrates of different stiffnesses, with a Young's modulus of 8.4 kPa or 20.7 kPa, or coated with different ligands, collagen I (CnI) or fibronectin (FN). Ligand biochemistry and gel stiffness indicated. Data reflects statistics as follows: FN, 8.4 kPa ($n = 18$ cell pairs); Cn I, 8.4 kPa ($n = 24$ cell pairs); Cn I, 20.7 kPa ($n = 15$ cell pairs). Statistical properties of data shown in box plot are as follows: mean (open square), box (25/75% quantile), whisker (5/95% quantile), and asterisks (maximum/minimum). (*B*) Box plot of cell–cell force for all three substrate conditions as in *A*. (*C*) Cell–cell force as a function of cell-ECM force for all three substrate conditions indicated: FN, 8.4 kPa (open green triangles); CnI, 8.4 kPa (closed red squares); CnI, 20.7 kPa (closed blue circles). Dashed line indicates a slope of 0.5.

mechanics of the ECM can significantly impact the endogenous forces at cell–cell contacts, but a robust correlation between the cell-ECM and cell–cell force remains.

Overall Forces Exerted by Cells in a Minimal Tissue with Disparate Microenvironments Are Similar. In epithelial sheets, cells toward the boundary sustain significant traction forces, but cells in the interior exert diminished traction forces at the cell-ECM interface (15). To consider the implications of our data to such multicellular arrangements, we considered an asymmetric case of three cells arranged in a linear fashion wherein the inner cell is bound by cell–cell adhesion on either side while all three cells have the opportunity to bind to ECM on their basal surface (Fig. 5 *A* and *B* and Fig. S5).

For both of the outer cells containing a single cell–cell contact, the cell–cell force is approximately 50% that of the total cell-ECM traction, similar to that observed in cell pairs (Fig. 5*C*). Furthermore, the absolute magnitudes of the cell–cell and cell-ECM forces were quite similar for the two outer cells, despite the fact that these cells did not share a common boundary (Fig. 5*C* and Fig. S5). By contrast, the inner cell exerted approximately 50% less traction on the ECM (Fig. 5 *A*–*C*). However, because this cell has two cell–cell contacts, this cell experienced approximately twice the tension through cell–cell contacts as do the boundary cells (Fig. 5*C*). Strikingly, the overall force that each of the three cells exerts on its microenvironment, measured as the sum of the cell–cell force magnitudes and traction force magnitudes, was similar for the inner and outer cells (Fig 5*C* and Fig. S5). Thus, even though the inner cell is more extensively bound by cell–cell adhesion and exhibits diminished cell-ECM traction forces, its mechanical interaction with its microenvironment is not diminished.

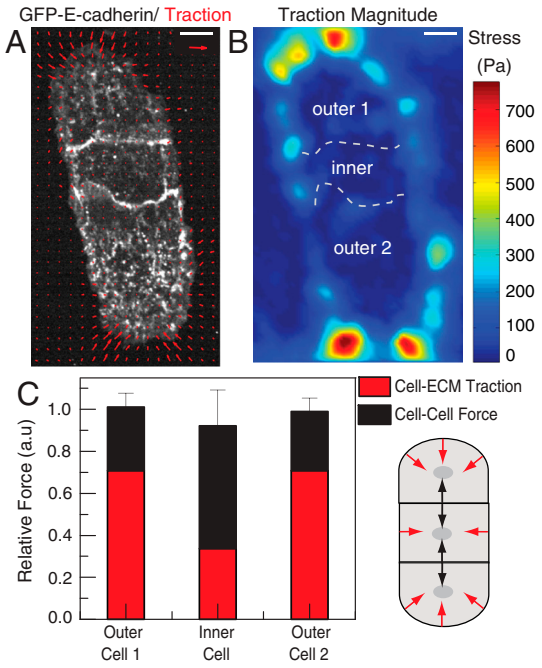

Fig. 5. *Total forces exerted on the microenvironment by individual cells in a linear three-cell island are similar.* (*A*) Traction stresses exerted by a linear three-cell island of MDCK cells expressing GFP-E-cadherin. Traction stress vectors are overlaid (red arrows). Reference traction vector is 1,000 Pa; scale bar indicates 10 μm. (*B*) Heat-scale map of the traction magnitude for the cell island shown in *A*. Dashed white line indicates cell–cell contacts. The three cells are indicated by text. (*C*) Relative total cell-ECM traction force (red) and cell–cell force (black) exerted by the three cells shown in *A*. Values are relative to the average between the total forces exerted by the outer cells. Schematic on the right depicts the three-cell configuration and the cell-ECM (red arrows) and cell–cell (black arrows) forces exerted by each cell. Data reflect the mean and standard deviation for $n = 4$ cell islands with identical geometry.

Discussion

Our paper provides quantitative estimates of the force exerted at a fully developed cell–cell contact between two epithelial cells that are free to dynamically modify their contact to the ECM as well as with each other. The forces exerted at these bonafide cell–cell contacts are not only substantial but also comparable in magnitude to traction forces measured at focal adhesions. Considering recent evidence that suggests that cadherin-based adhesions are sites of mechanosensation (8, 9), this implies that biochemical cues arising from mechanotransduction at cell–cell and cell-ECM contacts will both play significant roles in regulating cell physiology.

We find that the tension exerted at a cell–cell contact remains stable despite significant fluctuations in the shape of the cell pair as well as the length or shape of the cell–cell contact as the cells comigrated randomly on the ECM. The cell–cell force measured by TFIM is also uncorrelated with the integrated E-cadherin intensity at the cell–cell contact. This is in contrast to recent findings that reported a correlation of cell–cell force of endothelial cell pairs with junction size (16). However, cells in that study were plated on micropatterned ECM, which constrains cell shape and limits the extent of maximal contact between cells and range of traction forces observed. The impact of such geometric constraints on the forces reported is unclear. For instance, if the cell–cell force is concentrated at the vertices and acting in the direction of the cell edge, increase in cell–cell contact size of a bowtie-shaped cell pair would result in an increase in the component of cell–cell force that is normal to the cell–cell contact. As this is the component measured by TFIM, this would result in an apparent increase in the cell–cell force even if the total cell–cell force magnitude remains constant (16). It is important to note that our results do not preclude local correlations between tension and E-cadherin accumulation.

Our calcium depletion experiments further suggest that the force at the cell–cell contact in a cell pair is concentrated at the contact edges. This nonuniform distribution of force may explain the enhanced localization of E-cadherin observed as plaques at the contact edges of epithelial cell pairs as cadherin localization is known to be force dependent (8, 9). This also suggests that cadherins at the contact edges sustain greater forces and may be specialized zones of enhanced localized signaling in response to enhanced mechanical cues.

The ratio of the cell–cell force to the total cell-ECM force exerted by individual cells within cell pairs is remarkably constant. This result is insensitive to the methods used to reconstruct traction and calculate the forces (Figs. S6–S8 and Table S1). The constancy of this ratio is likely due to the commonality in biochemical cues that regulate the contractile state of the cell. We propose that a common actomyosin structural framework may provide a physical link that contributes to the coordinated mechanics at cell–cell and cell-ECM contacts demonstrated here, consistent with studies of cytoskeletal force transmission (25–27). In fact, such direct physical links between the junctions are apparent in cell pairs (Fig. S2) and are presumably mediated by a prestressed actin cytoskeleton (27). The magnitude of the ratio between cell–cell and cell-ECM forces is likely controlled by the specific geometry of the contact and the relative extent of cell–cell and cell-ECM contact, as we observed variations between cells in linear three-cell islands. For a given configuration, it remains to be understood what factors determine the relative extent of F-actin linkages to cell–cell and cell-ECM adhesions. For instance, differences in the mechanosensitivity and force dependence of cadherin- and integrin-based adhesions may guide changes in the force balance observed between cell–cell and cell-ECM traction forces.

Our results also show that biochemical and mechanical properties of the ECM alone can directly impact the force levels at cell–cell junctions. In development and disease, changes in ECM properties are known to influence the behaviors of multicellular tissue (28, 29); our results imply that part of this may be a consequence of altered tension at cell–cell interfaces. For instance, our results showing a strong correlation between cell–cell tension and cell-ECM tension shed light into the role of perturbed ECM mechanics in tumor progression (28, 30).

There are several implications of our results to forces at cell–cell contacts in more general two-dimensional multicellular assemblies, such as epithelial monolayers. Although we find that the cell–cell force is essentially normal to the contact for a cell pair, cell–cell forces in general 2D assemblies can be expected to have appreciable components in directions both normal and parallel to the cell–cell interface. Direct measurements of endogeneous cell–cell forces with these geometries will help establish a more solid mechanical footing to interpretations of cell–cell tensions made from laser ablation experiments inside tissue.

Our minimalistic tissue model consisting of a linear array of three cells reflects an important feature of monolayers wherein the outer cells exhibit enhanced traction forces and the inner cell, which is bound by more extensive cell–cell adhesion, exerts diminished traction on the ECM. If the traction forces on the outer cells were internally balanced, the inner cell would feel very little net tension and would be mechanically quiescent. However, instead, we find that the traction forces exerted by the outer cells are not balanced such that the inner cell experiences similar force levels to the cells on the periphery. Our data indicate each cell in a multicellular arrangement sustains a similar level of tension, with the magnitude of forces sustained at cadherin- and integrin-mediated adhesions changing depending on the geometry of adhesion. Thus, our data provide direct evidence of the mechanical coordination between cell-ECM and cell–cell adhesions. It is likely that a fine balance between forces sustained at these two types of adhesions exists to control tissue morphology and behavior.

Materials and Methods

MDCK cells stably expressing GFP-E-cadherin (20) were plated on collagen-coated polyacrylamide (PAA) gels suitable for traction force microscopy, as described in ref. 19. Further details of live cell imaging, traction force microscopy, and analysis are found in *SI Text*. Unless otherwise specified, cells were plated on PAA gels with a Young's modulus of 8.4 kPa coated with Collagen I.

ACKNOWLEDGMENTS. We thank James Nelson and Nicolas Borghi (Stanford University, Palo Alto, CA) for MDCK cells expressing GFP-E-cadherin and useful discussions. We thank Karl Matlin (University of Chicago, Chicago, IL) for MDCK cells expressing GFP-vinculin and useful discussions. M.L.G. acknowledges support from the National Institutes of Health (Grant DP10D00354), Packard Foundation, and a Burroughs Wellcome Career Award. U.S.S. acknowledges support from the cluster of excellence CellNetworks at Heidelberg and from the MechanoSys-grant from the Federal Ministry of Education and Research of Germany. V.M. acknowledges support from an American Heart Association Midwest Affiliate Postdoctoral Fellowship.

1. Paluch E, Heisenberg C-P (2009) Biology and physics of cell shape changes in development. *Curr Biol* 19:R790–R799.
2. Gumbiner BM (2005) Regulation of cadherin-mediated adhesion in morphogenesis. *Nat Rev Mol Cell Biol* 6:622–634.
3. Schwartz MA, DeSimone DW (2008) Cell adhesion receptors in mechanotransduction. *Curr Opin Cell Biol* 20:551–556.
4. Chen CS, Tan J, Tien J (2004) Mechanotransduction at cell-matrix and cell-cell contacts. *Annu Rev Biomed Eng* 6:275–302.
5. Gardel ML, Schneider IC, Aratyn-Schaus Y, Waterman CM (2010) Mechanical integration of actin and adhesion dynamics in cell migration. *Annu Rev Cell Dev Biol* 26:315–333.
6. Paul AJ, Jessamine PW, Maria EM, Qi W (2009) The hard life of soft cells. *Cell Motil Cytoskel* 66:597–605.
7. Discher DE, Janmey P, Wang Y-l (2005) Tissue cells feel and respond to the stiffness of their substrate. *Science* 310:1139–1143.
8. le Duc Q, et al. (2010) Vinculin potentiates E-cadherin mechanosensing and is recruited to actin-anchored sites within adherens junctions in a myosin II-dependent manner. *J Cell Biol* 189:1107–1115.
9. Ladoux B, et al. (2010) Strength dependence of cadherin-mediated adhesions. *Biophys J* 98:534–542.
10. Ganz A, et al. (2006) Traction forces exerted through N-cadherin contacts. *Biol Cell* 98:721–730.
11. Hutson MS, et al. (2003) Forces for morphogenesis investigated with laser microsurgery and quantitative modeling. *Science* 300:145–149.
12. Peralta XG, et al. (2007) Upregulation of forces and morphogenic asymmetries in dorsal closure during Drosophila development. *Biophys J* 92:2583–2596.
13. Rauzi M, Verant P, Lecuit T, Lenne P-F (2008) Nature and anisotropy of cortical forces orienting Drosophila tissue morphogenesis. *Nat Cell Biol* 10:1401–1410.
14. Fernandez-Gonzalez R, et al. (2009) Myosin II dynamics are regulated by tension in intercalating cells. *Dev Cell* 17:736–743.
15. Trepat X, et al. (2009) Physical forces during collective cell migration. *Nat Phys* 5:426–430.
16. Liu Z, et al. (2010) Mechanical tugging force regulates the size of cell-cell junctions. *Proc Natl Acad Sci* 107:9944–9949.
17. Tsai J, Kam L (2009) Rigidity-dependent cross talk between integrin and cadherin signaling. *Biophys J* 96:L39–L41.
18. de Rooij J, et al. (2005) Integrin-dependent actomyosin contraction regulates epithelial cell scattering. *J Cell Biol* 171:153–164.
19. Sabass B, Gardel ML, Waterman CM, Schwarz US (2008) High resolution traction force microscopy based on experimental and computational advances. *Biophys J* 94:207–220.
20. Adams CL, Chen Y-T, Smith SJ, James Nelson W (1998) Mechanisms of epithelial cell–cell adhesion and cell compaction revealed by high-resolution tracking of E-cadherin–green fluorescent protein. *J Cell Biol* 142:1105–1119.
21. Yamada S, Nelson WJ (2007) Localized zones of Rho and Rac activities drive initiation and expansion of epithelial cell cell adhesion. *J Cell Biol* 178:517–527.
22. Shewan AM, et al. (2005) Myosin 2 is a key rho kinase target necessary for the local concentration of E-cadherin at cell-cell contacts. *Mol Biol Cell* 16:4531–4542.
23. Meza I, et al. (1980) Occluding junctions and cytoskeletal components in a cultured transporting epithelium. *J Cell Biol* 87:746–754.
24. Ohashi T, Ichihara H, Sakamoto N, Sato M (2009) Specify of traction forces to extracellular matrix in smooth muscle cells. *IFMBE Proc* 23:1–2.
25. Hu S, et al. (2003) Intracellular stress tomography reveals stress focusing and structural anisotropy in cytoskeleton of living cells. *Am J Physiol-Cell Ph* 285:C1082–1090.
26. Cai Y, et al. (2010) Cytoskeletal coherence requires myosin-IIA contractility. *J Cell Sci* 123:413–423.
27. Wang N, et al. (2002) Cell prestress. I. Stiffness and prestress are closely associated in adherent contractile cells. *Am J Physiol-Cell Ph* 282:C606–616.
28. Paszek MJ, et al. (2005) Tensional homeostasis and the malignant phenotype. *Cancer Cell* 8:241–254.
29. Guo WH, Frey MT, Burnham NA, Wang YL (2006) Substrate rigidity regulates the formation and maintenance of tissues. *Biophys J* 90:2213–2220.
30. Levental KR, et al. (2009) Matrix crosslinking forces tumor progression by enhancing integrin signaling. *Cell* 139:891–906.